Xiaoqiang Liu[a], Chun Zhou[a], Honggang Xia*, Yang Zhou* and Weidong Jiang

Dissipative particle dynamics simulation on the self-assembly of linear ABC triblock copolymers under rigid spherical confinements

DOI 10.1515/epoly-2016-0306
Received November 23, 2016; accepted December 22, 2016; previously published online January 23, 2017

Abstract: Although a great deal of unique nanostructures were already obtained from polymer self-assemblies in terms of conventional parameters, the self-assembly under the confinement is still not well understood. Here, dissipative particle dynamics simulations were used to explore the self-assemble behaviors of linear ABC triblock copolymers under rigid spherical confinements. First several unusual morphologies, such as multilayer onion, coupled helix, and stacked lamella, were distinguished from the total 210 simulations. Second, the influences of three important parameters (block sequence, wall selectivity, and spherical radius) on the morphologies were discussed in detail. Finally, the dynamics evolution of several typical aggregates was examined. This simulation enriches micelle morphologies for the self-assembly of linear ABC triblock copolymers under rigid spherical confinements and is helpful to understand the formation of valuable nanostructures from linear ABC terpolymers.

Keywords: computer simulation; DPD; self-assembly; spherical confinement; triblock copolymer.

1 Introduction

Rich nanostructures from the self-assembly of block copolymers (BCPs) have gained tremendous scientific interests because of their potential applications, such as in drug delivery, microelectronic materials, advanced plastics, and so on (1–4). Recently, it was reported that the confined assembly of BCPs can provide a powerful strategy to manipulate the shape and internal structure of nanomaterials (5–18). Considering the key role of shape and internal structure in the function of polymer particles, how to systemically control their morphologies is still of great significance. However, confined spaces unavoidably introduce new parameters, such as space size, shape, and wall selectivity, to influence the morphology of BCPs, which brings the tremendous challenge for experimental works. In fact, the simulation techniques are the good supplement. Recently, we have successfully used dissipative particle dynamics (DPD) simulations to explore the self-assemble behavior of linear ABC (l-ABC) triblock copolymers in the dilute solution and shear condition (19, 20). Here, we continually utilized DPD methods to investigate the self-assembly of linear ABC terpolymers in three-dimensional (3D) spherical confinements.

Then we briefly summarized recent experimental and simulation works on the assembly of BCPs in confined spaces. Experimentally, in the one-dimensional (1D) confinement, Ludwigs et al. (21) found highly ordered hexagonal perforated lamella from the self-assembly of poly(*tert*-butyl methacrylate)-poly(2-vinylpyridine)-polystyrene triblock copolymers. Tang et al. (22) found half-sphere, half-sphere plus whole sphere, half-sphere plus two whole sphere, and coexistence of regions of hexagonal and square packing from the triblock copolymer of poly(ethylene oxide)-poly(methyl methacrylate)-polystyrene. In the two-dimensional (2D) cylindrical confinement, Dobriyal et al. (23) observed concentric cylinders, single-, double-, triple-helical, and torus-like morphologies from polystyrene-polybutadiene diblock copolymers. In the 2D confinements (spherical or polyhedral), Arsenault et al. (24) investigated the self-assembly of polystyrene-poly(ferrocenylethylmethylsilane) diblock copolymer and predicted the lamellae orthogonal to the sphere surface because of the strong confined influence. Xu et al. (25) studied the self-assembly of polystyrene-polyisoprene-poly(2-vinylpyridine) terpolymers and found several novel nanostructures, including pupa-like, core-shell, and onion-like stuctures. The more works can refer to the review by Yabu and coworkers (26).

On the other hand, a series of theoretical methods, including Monte Carlo (MC), simulated annealing,

[a]These authors contributed equally to this work.

***Corresponding authors: Honggang Xia,** The First Affiliated Hospital of Dalian Medical University, 116000 Dalian, China, e-mail: xia_honggang@126.com; and **Yang Zhou,** Institute of Chemical Materials, Chinese Academy of Engineering and Physics, 621900 Mianyang, China, e-mail: zhouy@caep.cn
Xiaoqiang Liu and Weidong Jiang: College of Chemistry and Environmental Engineering, Sichuan University of Science and Engineering, Zigong 643000, China
Chun Zhou: Institute of Chemical Materials, Chinese Academy of Engineering and Physics, 621900 Mianyang, China

self-consistent field theory (SCFT), DPD, and so on, were utilized to explore the self-assembly of BCPs. For example, Geisinger et al. (27) studied the self-assembly of symmetric diblock copolymers by using SCFT and MC simulations under 1D confinement. Yang et al. (28) used real-space SCFT to search possible morphology of an asymmetric diblock copolymer confined in two homogeneous hard walls and found several interesting structures, including parallel cylinder, perpendicular cylinder, flat lamellae, undulated cylinders, and lamellae. Ludwigs et al. (21, 29) coarsed polystyrene-poly(2-vinylpyridine)-poly(tertbutylmethacrylate) triblock copolymers as Gaussian chain of A3B4C12 and used SCFT methods to systematically explore the influence of film thickness, surface field, and interaction parameters between the different polymer components on the phase behavior. Chen and Fredrickson (30) also used the same method to investigate symmetric ABC terpolymers confined in thin film conditions and predicted parallel and perpendicular cylinders. Moreover, Li et al. (31) applied SCFT method to study the assembly of symmetric ABC star terpolymers in spherical cavity. Spherically concentric lamellae and ringlike structures were also observed in their study. Arai et al. (32) utilized DPD simulations to study the self-assembly of Janus nanoparticle of ABC terpolymers under nanotube confinement and gained double-helix and triple-helix nanostructures. Chi et al. (33) have systematically investigated the self-assembly of diblock copolymers under soft confinements by simulated annealing methods. Based on MC methods, Sheng et al. (34) studied the self-assembly of ABA terpolymer in 3D confinements and observed double-helixes, stacked rings, and cagelike morphologies. By DPD simulations, Chang et al. (35) studied the phase behaviors of confined linear triblock copolymers and found that helical nanostructures can be induced by blending non-helix-forming terpolymers with homopolymers or diblock copolymers.

Although a lot of experimental and theoretical works have been performed, it is clear that the self-assembly of linear ABC triblock copolymers in 3D rigid confinement (spherical cavity) is still rare. In our previous study, we explored the morphology of linear ABC triblock copolymers under the shear rate, solutions, and different block sequences by DPD simulations (19, 20, 36). Here, we further utilized DPD simulations to investigate the self-assembly of linear ABC triblock copolymers in rigid spherical confinements.

2 Simulation details

DPD is a coarse-grained simulation technique, such as the common molecular dynamics (MD), however, which allows the larger length and longer time scale (37). Coarse-grained particles in DPD represent a block or cluster of atoms or molecules, and their evolutions obey Newton's equation of motion. The force between pair nonbonded DPD particles includes a conservative force F_{ij}^C, a dissipative force F_{ij}^D, and a random force F_{ij}^R, respectively. Bonded DPD particles are described by a harmonic spring force F_{ij}^S. Therefore, all the forces are expressed by

$$f_i = \sum_{i \neq j} (F_{ij}^C + F_{ij}^D + F_{ij}^R + F_{ij}^S) \quad [1]$$

$$F_{ij}^C = -\alpha_{ij} w^C(r_{ij}) \mathbf{e}_{ij} \quad [2]$$

$$F_{ij}^D = -\gamma w^D(r_{ij})(\mathbf{e}_{ij} \cdot \mathbf{V}_{ij}) \mathbf{e}_{ij} \quad [3]$$

$$F_{ij}^R = \sigma w^R(r_{ij}) \xi_{ij} \Delta t^{0.5} \mathbf{e}_{ij} \quad [4]$$

$$F_{ij}^S = -\sum_{j=i+1} k_s (l_{ij} - l_0) \quad [5]$$

where $\mathbf{r}_{ij} = \mathbf{r}_i - \mathbf{r}_j$, $r_{ij} = |\mathbf{r}_{ij}|$, $\mathbf{e}_{ij} = \mathbf{r}_{ij}/r_{ij}$, and $\mathbf{v}_{ij} = \mathbf{v}_i - \mathbf{v}_j$. ξ_{ij} is a Gaussian random number with zero mean and unit variance. α_{ij} is the repulsion parameter between bead i and j, which reflects the chemical characteristics of interacting beads. γ is the friction constant, and σ is the noise strength. To ensure the simulation system to satisfy the fluctuation-dissipation theorem and the Gibbs Canonical ensemble, only one of the two weight functions w^D and w^R can be chosen arbitrarily and this choice fixes the other one. There is also a relation between amplitudes (σ and γ) and k_BT. It is $w^D = (w^R)^2$ and $\sigma^2 = 2\gamma k_B T$, where k_B is the Boltzmann constant and T is the temperature (38). Generally, the simple forms for $w^C = w^D = (w^R)^2 = (1 - r_{ij})^2$ and $\sigma = 3$ (i.e. $\gamma = 4.5$) are chosen, and Newton equations for all paritcles are integrated by a modified version of the velocity-Verlet algorithm with $\lambda = 0.65$ (39). l_{ij} is the bond length between connected two bead i and j. Here, the spring coefficient $k_S = 4$ and the balance bond length $l_0 = 0$ are chosen. For easy numerical handling, the cutoff radius (r_c), the bead mass (m), and the temperature (k_BT) are chosen as the unit of the simulated system.

In this work, the morphology of linear ABC triblock copolymers confined in a 3D spherical cavity is investigated. As shown in Figure 1a, *l*-ABC, *l*-BAC, and *l*-ACB consist of A, B, and C blocks according to the different sequences, x, y, and z denote A block with x beads, B block with y beads, and C block with z beads, respectively. The cavity wall is also constructed by DPD beads (denoted by W), and the radius $\boldsymbol{R}$ of the spherical cavity is chosen as 60 and 80 in DPD unit (Figure 1b). In detail, the cavity wall is

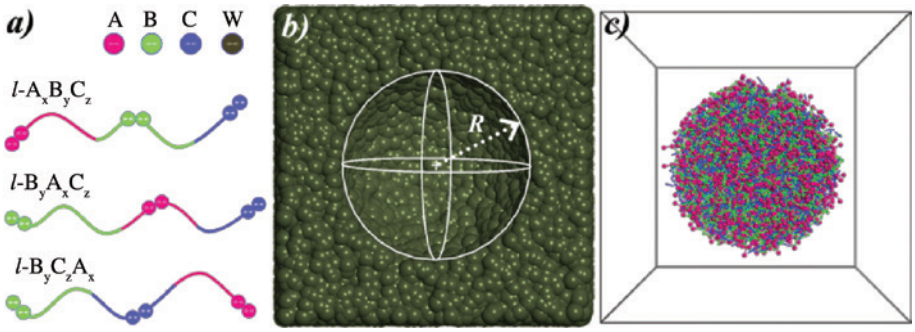

Figure 1: The coarse-grained model of linear ABC triblock copolymers with different block sequences (a), the spherical cavity (b), and the simulation box with the initial constitution (c).

modeled by a set of fixed W beads, which are placed randomly with the high number density of $\rho = 6$ for preventing the transmission of BCPs. Triblock copolymers are stuffed into the spherical cavity with random distribution at $\rho = 3$. The repulsive parameters in Table 1 for the conservative force between DPD particles still follow those used by our previous works (19, 36, 40), which are defined to describe the self-assembly of the experimental miktoarm terpolymers (41). Note that A, B, and C-blocks are incompatible to one another and α_{iW} depicts the interaction between bead *i* and the cavity wall (W). In the initial stage, B-blocks are absolutely abstracted by the wall, and C-blocks are strongly repelled from the wall. Afterward, the additional parameters of $\alpha_{AS} = 25$ and 120, $\alpha_{BS} = 120$, and $\alpha_{CS} = 25$ are also chosen to check the influence of α_{iW} on the morphologies of linear ABC terpolymers. In this work, the time step $\Delta t = 0.04$ is chosen to obtain the better control of the temperature fluctuation of simulation systems, and a total of 2×10^6 DPD steps are carried out to guarantee the equilibration for each system.

Table 1: Repulsion parameters α_{ij} (DPD unit) in this work.

α_{ij}	A	B	C	W
A	25			
B	45	25		
C	90	75	25	
W	50 (25, 120)	25 (120)	120 (25)	25

3 Results and discussions

Clearly, the morphology of linear ABC triblock copolymers in 3D rigid confinements (spherical cavity) is influenced by a series of controlling parameters, such as block sequences (ABC, BAC, and BCA), interactions between terpolymers and wall of cavity (α_{iW}), block lengths (*x*, *y*, *z*), the radius of spherical cavity (***R***), and so on. Considering the combination of the different parameters, they constitute a tremendous parameter space. It is not possible to explore the effect of all the factors. Hence, we first fixed the interactions between different blocks, that is, α_{AB}, α_{AC}, and α_{BC} (see Table 1). Then we also considered the variation of other parameters, including three block sequences (*l*-ABC, *l*-BAC, and *l*-BCA), seven block lengths (*x*-*y*-*z* is equal to 2-2-2, 2-2-8, 2-8-2, 2-2-8, 8-2-2, 8-2-8, and 8-8-2, respectively), two radii of rigid spherical cavity ($\boldsymbol{R} = 60$ and 80), and five sets of α_{iW} ($\alpha_{AW} = 50$, $\alpha_{BW} = 25$, $\alpha_{CW} = 120$; $\alpha_{AW} = 25$, $\alpha_{BW} = \alpha_{CW} = 120$; $\alpha_{BW} = 25$, $\alpha_{AW} = \alpha_{CW} = 120$; $\alpha_{CW} = 25$, $\alpha_{AW} = \alpha_{BW} = 120$; and $\alpha_{AW} = \alpha_{BW} = \alpha_{CW} = 120$). In summary, there are a total of 210 simulations that are considered in this work.

3.1 Block sequence

Generally, the effect of block sequence on morphologies for multiblock copolymers is vital. Therefore, the morphology for linear ABC terpolymers with three difference sequences (A-B-C, B-A-C, and B-C-A) is examined under the following stationary conditions. Two sets of parameters for the selectivity of confined wall are fixed as $\alpha_{AW} = 50$, $\alpha_{BW} = 25$, $\alpha_{CW} = 120$, and $\alpha_{AW} = \alpha_{BW} = \alpha_{CW} = 120$, respectively. The interaction parameters between different blocks are listed in Table 1. The radius of spherical cavity is $\boldsymbol{R} = 60$. First Figure 2 gives a series of morphologies from symmetrical $A_2B_2C_2$, $B_2A_2C_2$, and $B_2C_2A_2$ triblock copolymers at two sets of interaction parameters (α_{iW}). As for $\alpha_{BW}(25) < \alpha_{AW}(50) < \alpha_{CW}(120)$ (Figure 2a), the sequence of B-A-C, that is, $B_2A_2C_2$, can result in the formation of a normal onion-like corona-shell-core (CSC) structure. In detail, blocks B, A, and C aggregate into the corona, shell, and core, respectively. After exchanging the position of

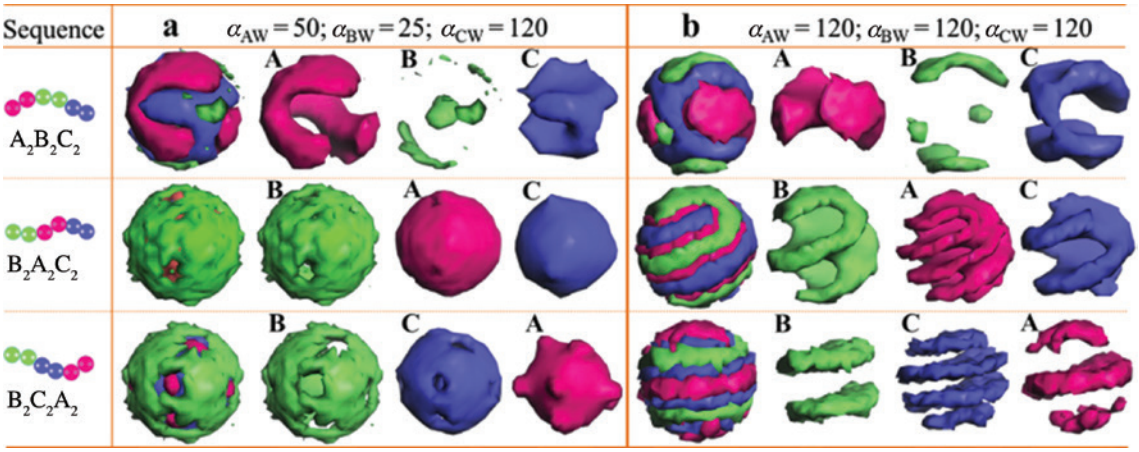

Figure 2: Simulation morphologies for symmetrical $A_2B_2C_2$, $B_2A_2C_2$, and $B_2C_2A_2$ triblock copolymers under two sets of interaction parameters of α_{iW} as a function of block sequences. Pink, green, and blue represent A-, B-, and C-rich domains, respectively.

blocks A and C, $B_2C_2A_2$ still aggregates into the normal CSC structure. The only difference is that the porous shell is from block C and the salient core is from block A. When block B is placed in the middle, that is, $A_2B_2C_2$, the CSC structure disappears which replaced by coupling striped patterns from blocks A and C. It is interesting that block B forms the small core away from the confined wall, although the wall is partial to block B. Then the parameters of $\alpha_{BW}=\alpha_{AW}=\alpha_{CW}=120$ (Figure 2b) are used to weaken the effect of wall selectivity, in this way, blocks A, B, and C have the equal chance to form the inner core, in order to avoid the contact with the wall. The diagonal of Figure 2b clearly shows the different morphologies of block A, that is, the irregular core for $A_2B_2C_2$, the helical structure for $B_2A_2C_2$, and the lamella for $B_2C_2A_2$. Under the condition of $\alpha_{BW}=\alpha_{AW}=\alpha_{CW}=120$, the effect of wall selectivity is eliminated; therefore, it thoroughly shows the effect of block sequences. Outwardly, the block sequence of block B in one end (B-A-C and B-C-A) can result in the similar morphologies, as compared with the other sequence of B in the middle (A-B-C). It is worth to note that the interaction parameters between different blocks ($\alpha_{AB}=45$, $\alpha_{BC}=75$, and $\alpha_{AC}=90$) also enter for the characteristic of morphologies.

For several asymmetric triblock copolymers, we also compared the variation of morphologies caused by block sequences, and the results are depicted in Figure 3. Similarly, the discussion still begins with the first parameters of $\alpha_{BW}(25)<\alpha_{AW}(50)<\alpha_{CW}(120)$. In Figure 3a, $A_8B_8C_2$ and $B_8A_8C_2$, with the position exchange of blocks A and B, show an interesting phenomenon, that is, the morphology of the exchanged blocks A and B has hardly any variation, and that of block C changes from several inlaid small dots to a whole core. The similar phenomenon is also found for $A_2B_8C_8$ and $A_2C_8B_8$ with the position exchange of B and C. $B_2A_8C_8$ and $B_2C_8A_8$ exhibit a slightly difference after switching the place of A and C. Block B actually becomes a core ($B_2C_8A_8$) from a corona ($B_2A_8C_8$). However, blocks A and C still occur a visible change, that is, a cage of block A around a polyhedral core of block C in $B_2A_8C_8$ and the coupled blocks A and C. So we can know that the hydrophilic B can bring complex variations if it is short and at the end.

The second parameters of $\alpha_{BW}=\alpha_{AW}=\alpha_{CW}=120$ (Figure 3b) are also chosen to remove the effect of wall selectivity. First by comparing Figure 3a and b, the variation of block sequences under this set of interaction parameters brings the entirely different morphological evolution. Taking $A_8B_8C_2$ and $B_8A_8C_2$ as an example, blocks A and B exchange the position and, meanwhile also switch their morphological structures. It is different with the above-mentioned situation that they retained the respective morphological characteristic after exchanging the position. If we neglect the small fluctuation of morphologies caused by the different block interactions (i.e. α_{AB}, α_{BC}, and α_{CA}), the similar conclusion can be obtained from $A_2B_8C_8$, $A_2C_8B_8$, $B_2A_8C_8$, and $B_2C_8A_8$.

3.2 Wall selectivity

Besides block sequences, the selectivity of confined wall also plays a significant role for the self-assembly under confined spaces. Combined with the fixed other parameters, we then tuned the parameter of α_{iW} to build the different wall selectivity, which includes $\alpha_{AW}=25$, $\alpha_{BW}=\alpha_{CW}=120$ (means the wall prefers block A to other two blocks, defined as AW), $\alpha_{BW}=25$ $\alpha_{AW}=\alpha_{CW}=120$ (liking block B, BW), and $\alpha_{CW}=25$ $\alpha_{AW}=\alpha_{BW}=120$ (liking block C, CW), as

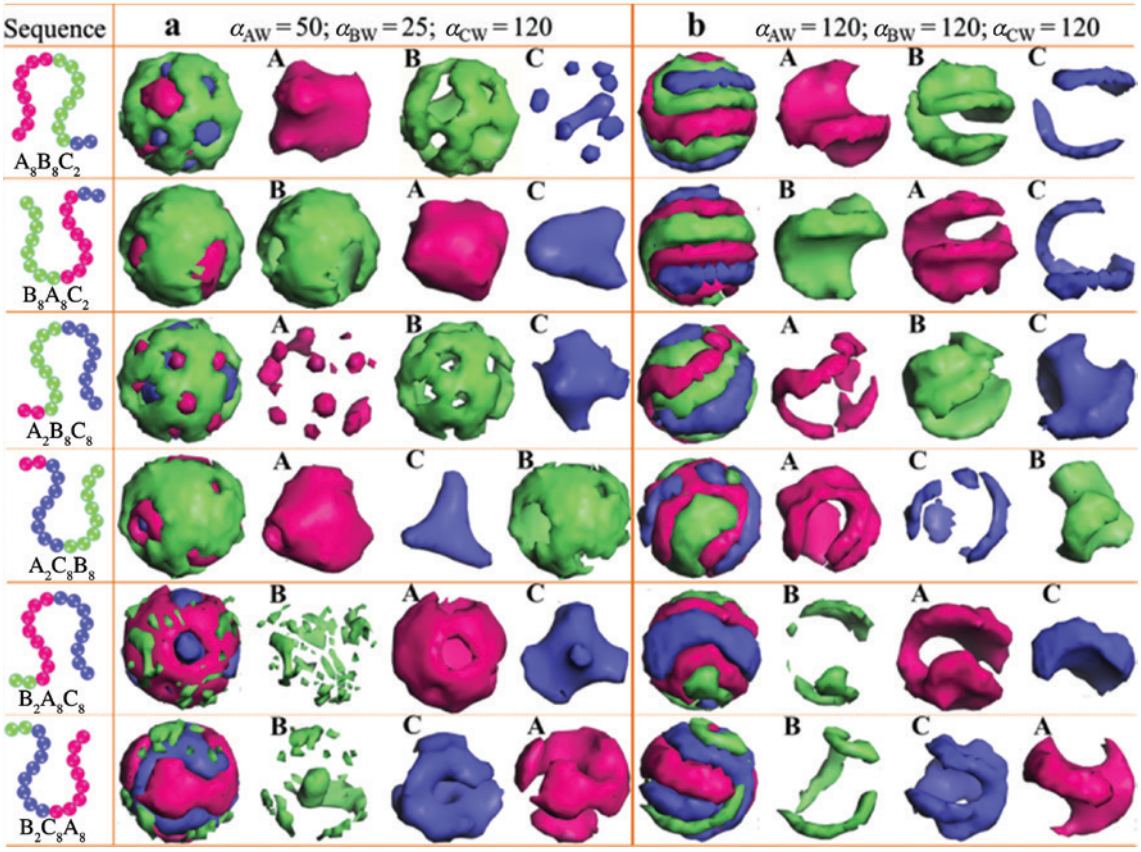

Figure 3: Simulation morphologies for asymmetrical $A_8B_8C_2$ and $B_8A_8C_2$, $A_2B_8C_8$ and $A_2C_8B_8$, $B_2A_8C_8$ and $B_2C_8A_8$ triblock copolymers under two sets of α_{iW} as a function of block sequences. Pink, green, and blue represent A-, B-, and C-rich domains, respectively.

shown in Figures 4–6. In fact, the different block lengths are also considered when building the phase diagrams for all linear ABC triblock copolymers. Therefore, the following discussion also includes the effect of block lengths.

Figure 4 first shows morphologies of all *l*-ABC terpolymers (2-2-2, 2-2-8, 2-8-2, 2-8-8, 8-2-2, 8-2-8, 8-8-2) in the rigid spherical cavity with $\boldsymbol{R}=60$. On the whole, *l*-ABC terpolymers prefer to form the CSC structure, except for those at the second selectivity of BW. In other words, if the block liked by the confined wall locates in the middle of ABC terpolymers, they would generally possess the larruping rule of morphological variation. For instance, the morphologies of *l*-$A_2B_2C_2$, *l*-$A_2B_8C_2$, and *l*-$A_8B_2C_8$ at the first selectivity (AW) are similar to those at the third selectivity (CW), but very different to those at the second one (BW). In detail, for *l*-$A_8B_2C_8$ of AW parameters, block A forms the multiporous corona, block B forms the stripped shell, and block C aggregates the irregular core. For the same polymer, the wall selectivity of CW parameters can simply exchange the morphologies of blocks A and C and hardly alter the morphology of B. However, for BW parameters, the morphology, a patch of block C is sewn on block A by a string of block B, is far away from the normal CSC structure. In fact, block B with the good wall selectivity does not form the corona because it is too short compared with the other two blocks. For *l*-$A_2B_8C_2$ of BW parameters, the longer B block is easier to build the cagelike corona of imprisoning several small spheres such as "fish" formed by blocks A and C.

As for all *l*-$B_yA_xC_z$ and *l*-$B_yC_zA_x$ triblock copolymers, the influence of the different wall selectivity on the morphology is also investigated, as drawn in Figures 5 and 6, respectively. Theoretically, the law of the two types of terpolymers should be similar to that of *l*-$A_xB_yC_z$. In Figure 5, $B_2A_2C_2$ assembles the normal CSC structure at both BW and CW parameters and the coupled double-helix at AW parameters. *l*-$B_8A_2C_8$ aggregates two helical strips from the longer blocks B and C that are sewn by the shorter block A. This morphology is very different to the CSC structures with the distinctly corona and core, which corresponds to the different BW and CW parameters, respectively. In addition for *l*-$B_2A_8C_2$, the selectivity of AW parameters also brings an A-cage entangling several B- and C-"fishes". Here, we can ensure that the law of wall selectivity shown by *l*-$B_yA_xC_z$ is consistent with that by *l*-$A_xB_yC_z$. In Figure 6, for symmetric *l*-$B_2C_2A_2$, the selectivity of AW and BW parameters only can exchange the corona and core of CSC

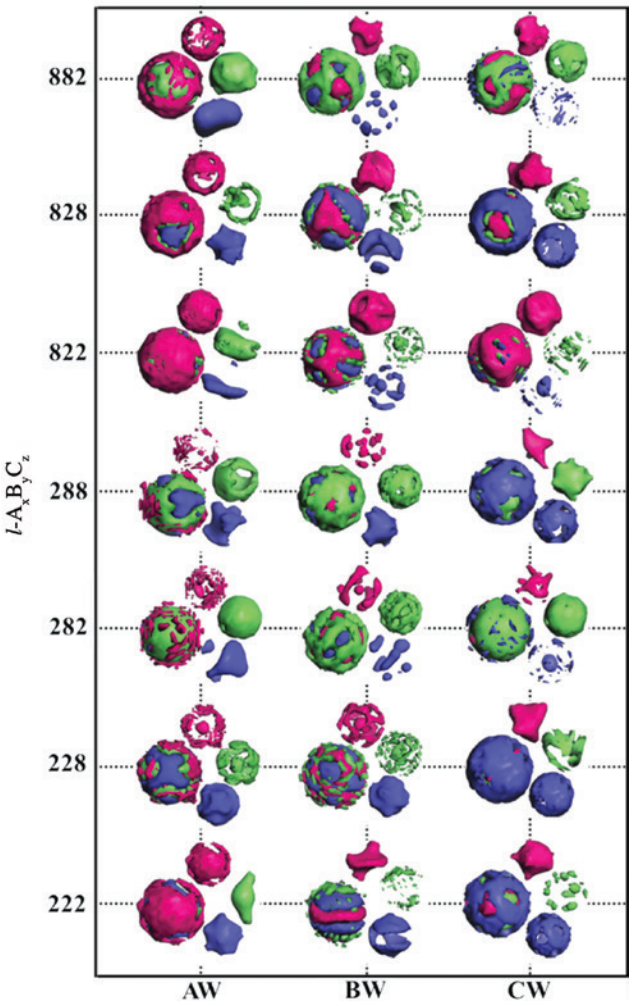

Figure 4: Morphologies for all *l*-ABC triblock copolymers at $\alpha_{AW}=25$, $\alpha_{BW}=\alpha_{CW}=120$ (defined as AW), $\alpha_{BW}=25$ $\alpha_{AW}=\alpha_{CW}=120$ (BW), and $\alpha_{CW}=25$ $\alpha_{AW}=\alpha_{BW}=120$ (CW). Pink, green, and blue represent A-, B-, and C-rich domains, respectively.

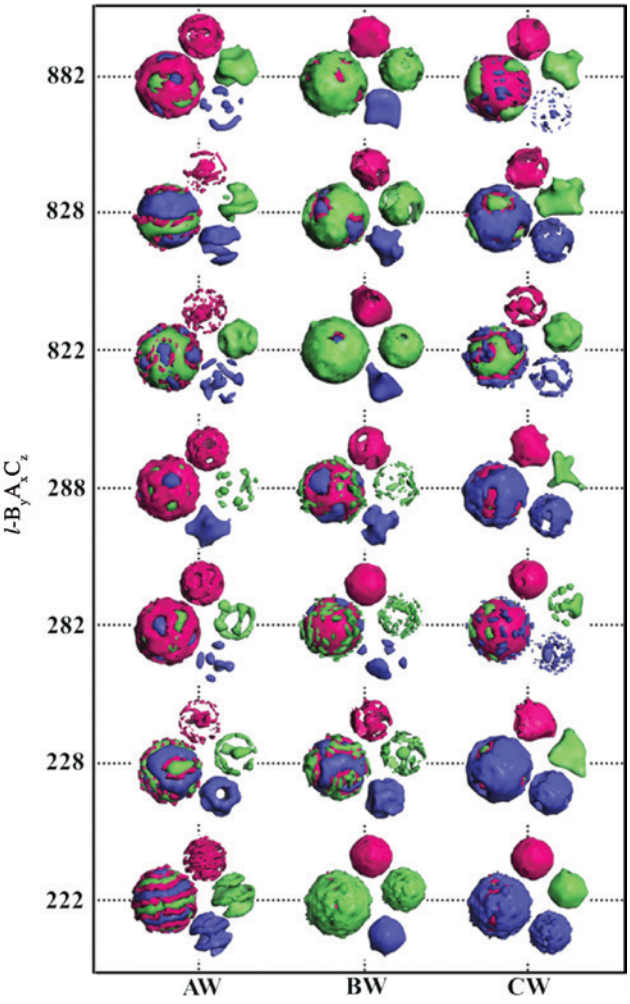

Figure 5: Morphologies for all *l*-BAC triblock copolymers at $\alpha_{AW}=25$, $\alpha_{BW}=\alpha_{CW}=120$ (AW), $\alpha_{BW}=25$ $\alpha_{AW}=\alpha_{CW}=120$ (BW), and $\alpha_{CW}=25$ $\alpha_{AW}=\alpha_{BW}=120$ (CW). Pink, green, and blue represent A-, B-, and C-rich domains, respectively.

structures. The selectivity of CW parameters results in a rambling CSC aggregate, which is different with the helix formed by l-$A_2B_2C_2$ and l-$B_2A_2C_2$. The reason may be the asymmetrical block interactions, and block C has the large repulsive characteristic with blocks A and B. However, for the asymmetric l-$B_2C_8A_2$ and l-$B_8C_2A_8$, the effect of asymmetrical block interactions seems lost, and we still find the similar morphological evolution with other two types of terpolymers. Therefore, we do not describe the morphological details again.

3.3 Spherical radius

In the previous sections, we examined the effect of block sequence and wall selectivity. Here, the effect of radius of confined spherical cavity on self-assembled morphologies is considered. Two kinds of radii are used, that is, $\boldsymbol{R}=60$ and 80. The corresponding morphologies for $\boldsymbol{R}=60$ have been seen in Figures 2 and 3, and those for $\boldsymbol{R}=80$ are shown in Figures 7 and 8 for comparisons.

We first compared the morphological diversity of symmetric terpolymers in Figures 2 and 7, respectively. In $\boldsymbol{R}=60$ (Figure 2a), l-$B_2A_2C_2$ forms the normal CSC structure when $\alpha_{AW}=50$, $\alpha_{BW}=25$, and $\alpha_{CW}=120$. However, when spherical radius increases from 60 to 80, its morphology shows a slight difference, as shown in Figure 7a. The routine corona becomes more scattered, and extra core also becomes the bigger than that in $\boldsymbol{R}=60$. Besides, the A-shell and C-core also grow many porous. The previous phenomenon is also found for l-$B_2C_2A_2$. l-$A_2B_2C_2$ for $\boldsymbol{R}=80$ (Figure 7a) has the thinner coupled strips than that for

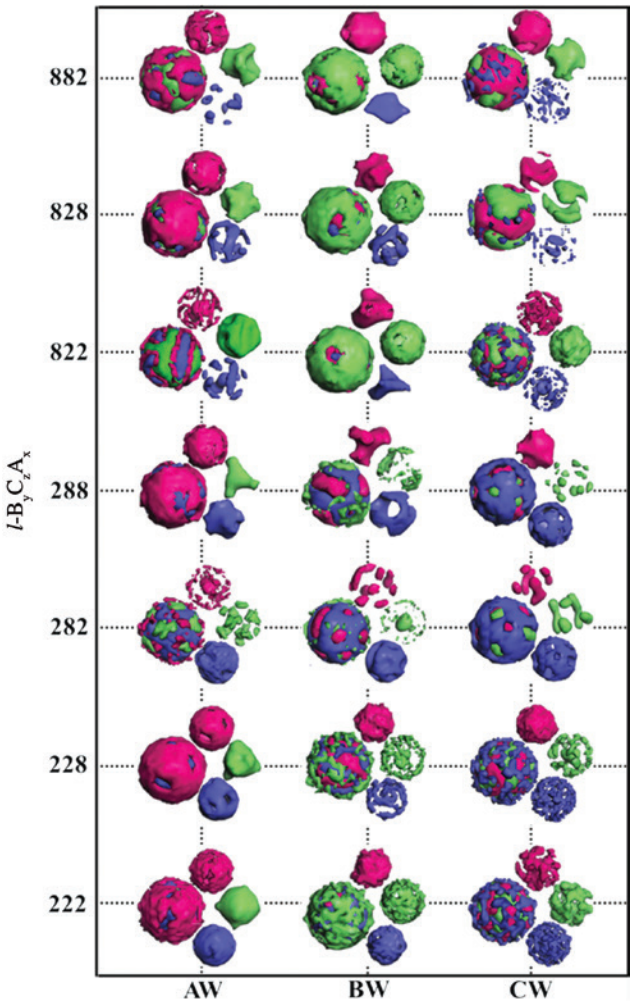

Figure 6: Morphologies for all l-BCA triblock copolymers at $\alpha_{AW}=25$, $\alpha_{BW}=\alpha_{CW}=120$ (AW), $\alpha_{BW}=25$ $\alpha_{AW}=\alpha_{CW}=120$ (BW), and $\alpha_{CW}=25$ $\alpha_{AW}=\alpha_{BW}=120$ (CW). Pink, green, and blue represent A-, B-, and C-rich domains, respectively.

$\boldsymbol{R}=60$ (Figure 2a). In Figure 7b ($\alpha_{AW}=\alpha_{BW}=\alpha_{CW}=120$), all three symmetric terpolymers form the coupled and independent helix that look like lamella from the whole morphology. Although Figure 2b shows a real lamella for l-$B_2A_2C_2$, and the thick strips with a little link for l-$A_2B_2C_2$, from the angle of the whole morphology, we can still think that when $\alpha_{AW}=\alpha_{BW}=\alpha_{CW}=120$, the radius of spherical confinement does not obviously change the morphology of symmetrical ABC triblock copolymers.

Second we also analyze the morphological difference of asymmetric ABC triblock copolymers, as shown in Figures 3 and 8. When the wall selectivity is fixed at $\alpha_{AW}=50$, $\alpha_{BW}=25$, and $\alpha_{CW}=120$, for example, we can clearly find that the morphology of l-$B_8A_8C_2$ in $\boldsymbol{R}=80$ (Figure 8a) shows an obvious change by comparing that in $\boldsymbol{R}=60$ (Figure 3a). In detail, l-$B_8A_8C_2$ in $\boldsymbol{R}=60$ forms the normal CSC structure with the B-corona, A-shell, and C-core. However, when the radius increases from 60 to 80, block B becomes the corona to the irregular core (like a four-way connection), and blocks A and C become the cage shape that corresponds to the corona and the shell, respectively. The terpolymers of l-$A_8B_8C_2$, l-$A_2B_8C_8$, and l-$A_2C_8B_8$ also have the similar phenomena, as shown in Figure 8a. In addition, the morphology of l-$B_2C_8A_8$ also shows the distinct variation only for blocks A and C, that is, in $\boldsymbol{R}=60$ blocks A and C form the two occlusive strips; however, in $\boldsymbol{R}=80$, block A becomes an irregular core with several hump and block C develops into a cage. Only l-$B_2A_8C_8$ does not show the marked morphological variation. If the wall selectivity is fixed at $\alpha_{AW}=\alpha_{BW}=\alpha_{CW}=120$, l-$A_2B_8C_8$, l-$A_2C_8B_8$, and l-$B_2A_8C_8$ express the similar laws with the previously mentioned findings from l-$A_8B_8C_2$, l-$B_8A_8C_2$, and l-$A_2B_8C_8$. In detail, in $\boldsymbol{R}=80$ (Figure 8b) middle

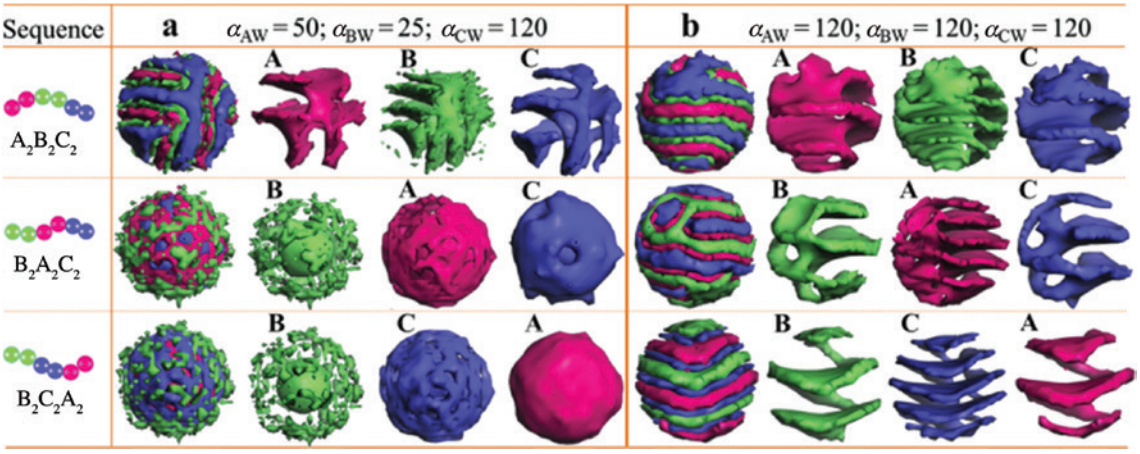

Figure 7: Morphologies of three symmetrical $A_2B_2C_2$, $B_2A_2C_2$, and $B_2C_2A_2$ terpolymers at $\boldsymbol{R}=80$. Pink, green, and blue represent A-, B-, and C-rich domains, respectively.

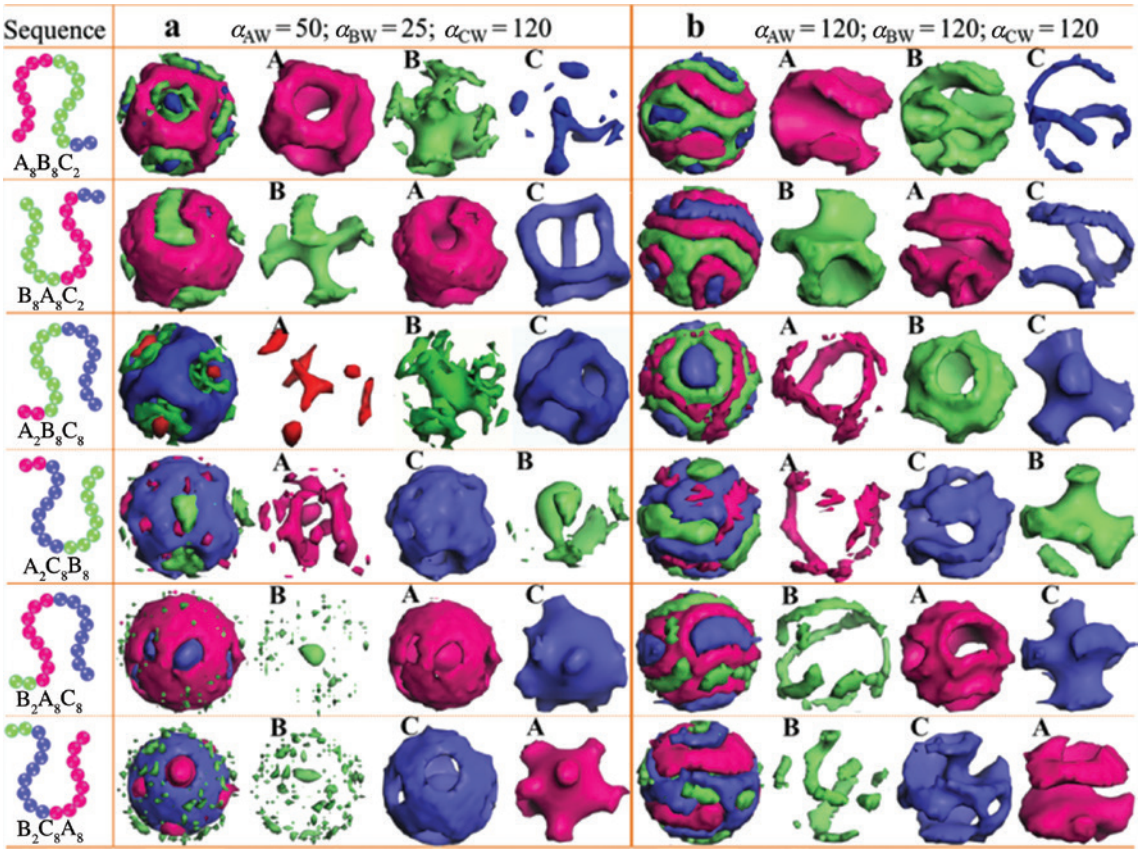

Figure 8: Morphologies of six asymmetrical $A_8B_8C_2$, $B_8A_8C_2$, $A_2B_8C_8$, $A_2C_8B_8$, $B_2A_8C_8$, and $B_2C_8A_8$ terpolymers at $\boldsymbol{R}=80$. Pink, green, and blue represent A-, B-, and C-rich domains, respectively.

blocks aggregate the cagelike structure that are different with those in $\boldsymbol{R}=60$ (Figure 3b). Other three terpolymers (l-$A_8B_8C_2$, l-$B_8A_8C_2$, and l-$B_2C_8A_8$) do not show the marked morphological variation under this repulsive wall selectivity and spherical radius. Again, we repeat our findings on the effect of spherical radius. The increase of radius of spherical confinement can significantly change the morphology of linear ABC triblock copolymers, especially for asymmetric block compositions and $\alpha_{AW}=50$, $\alpha_{BW}=25$, and $\alpha_{CW}=120$. Symmetrical block compositions are not easily influenced by the spherical radius, especially for the wall selectivity of $\alpha_{AW}=\alpha_{BW}=\alpha_{CW}=120$.

To further investigate the effect of spherical radius on the morphologies, we amply draw the inner structure of several CSC aggregates with similar appearance under the different spherical confinements by cutting them. The results are given in Figure 9a. As shown by ball-and-stick models in Figure 9a, l-$B_2A_2C_2$ in $\boldsymbol{R}=80$ forms the multilayer-onion structure with seven layers (that is BACABAC). However, the same terpolymer in $\boldsymbol{R}=60$ forms one with five layers (that is BACAB). The l-$B_2C_2A_2$ has the similar results, that is, it forms seven layers (BCACBCA) in $\boldsymbol{R}=80$ and five layers (BCACB) in $\boldsymbol{R}=60$, respectively. Obviously, the reason is that the fully expanded length of linear ABC triblock copolymers is still far less than spherical radius. Therefore, they cannot fill in the cavity of $\boldsymbol{R}=80$ by one chain, and need the relay of three chains (see Figure 9b). When the cavity decreases to $\boldsymbol{R}=60$, they only need the relay of two chain to fill in it (see Figure 9c). They clearly show the influence of the block length/spherical radius on the morphology. It is easy to think that increasing the block length can decrease the layers of multilayer onion aggregates. Hence, we also check the morphology of l-$B_2A_8C_8$ with longer blocks A and C in $\boldsymbol{R}=60$ and 80, respectively. The extended blocks A and C result in that the onion layers decrease from 7 to 5 in $\boldsymbol{R}=80$ and 5 to 3 in $\boldsymbol{R}=60$, respectively.

3.4 Dynamic evolution

Up to now, we have known the effect of block sequence, wall selectivity, and spherical radius on the assembled structures of linear ABC terpolymers. Furthermore, we

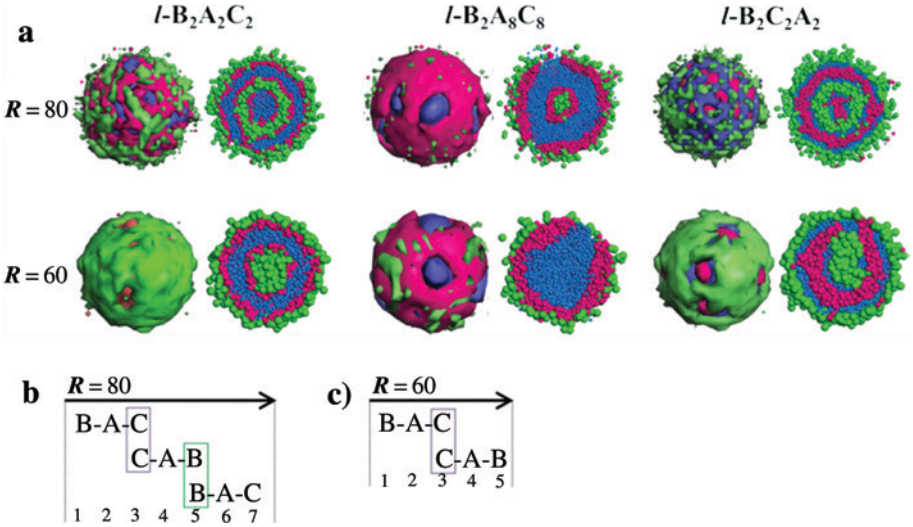

Figure 9: (a) Inner structures of several CSC aggregates with similar outward for the different spherical radius ($\boldsymbol{R}$ = 60 and 80) and α_{AW} = 50, α_{BW} = 25, and α_{CW} = 120. To clearly expression, the left inner structures are shown by the ball-and-stick model; (b) and (c) sketch maps for the distribution of ABC blocks. Pink, green, and blue represent A-, B-, and C-rich domains, respectively.

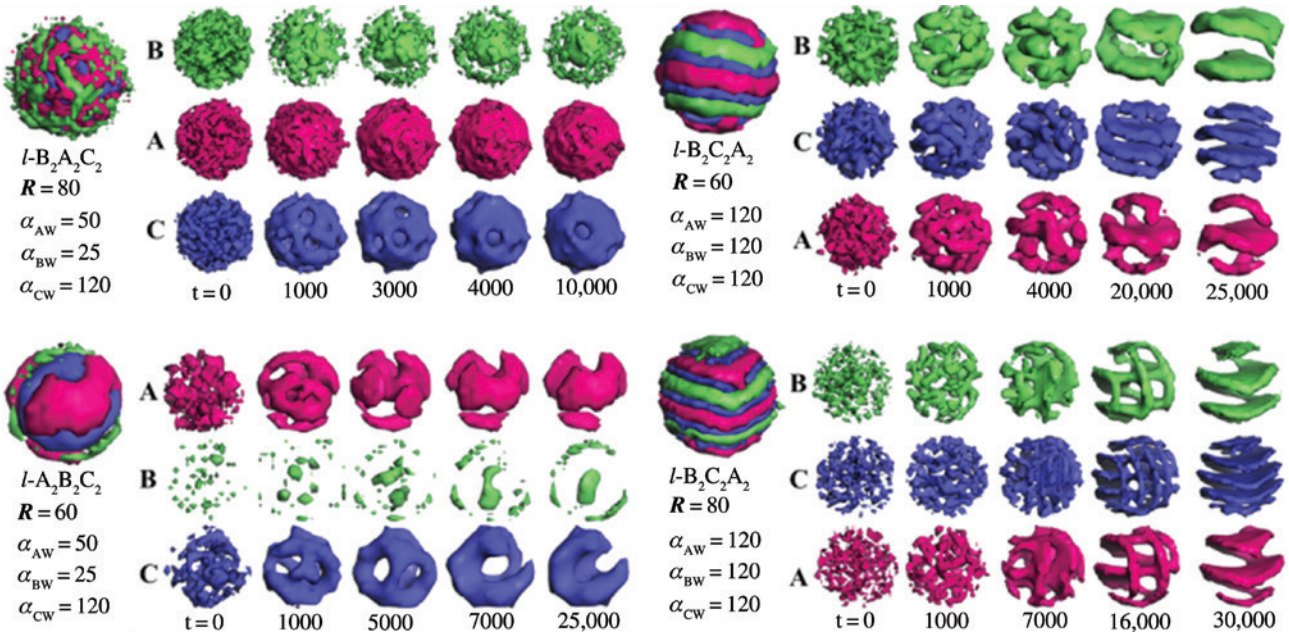

Figure 10: Dynamic evolution of $B_2A_2C_2$, $B_2C_2A_2$, and $A_2B_2C_2$ in the different parameter spaces. *t* is DPD steps. Pink, green, and blue represent A-, B-, and C-rich domains, respectively.

also found several typical morphologies, such as multilayer onion, lamella, helix, and so on. Then to seek the formation reason, we examine the dynamic formation pathways for these special aggregates.

For *l*-$B_2A_2C_2$ in $\boldsymbol{R}$ = 80 and α_{AW} = 50, α_{BW} = 25, and α_{CW} = 120, we have known its inner structure (Figure 9a). Here, we come to know the formation process. Figure 10 presents the separated dynamic evolution processes of A, B, and C domain, respectively. The microphase separation between blocks A, B, and C quickly appears at the primary stage of about t = 1000 DPD steps and becomes more and more striking when the simulation time increases. Clearly, block C begins to form a core except for the corona. Both A and C form a shell with several porous and gradually close. Finally, block A becomes an imperforate shell and B becomes a multiparous shell. Other onion-like structures also have the similar evolution process. In addition, we also find that the formative process of onion-like

structure is faster than others structures, and the time of self-assembly is generally less than $t = 10{,}000$ DPD steps. For l-$B_2C_2A_2$ in $\boldsymbol{R} = 60$ and $\alpha_{AW} = \alpha_{BW} = \alpha_{CW} = 120$, the early phase separation results in the formation of several small and dispersed lumps. Then the lump from same blocks begin to fuse and become big continuous regions ($t = 4000$ DPD steps). After $t = 20{,}000$, three blocks have begun to form the alternate independent phase that is the embryonic form of lamella. For the same terpolymer, when the spherical radius increases to $\boldsymbol{R} = 80$, the formation pathway is very similar to the stacked lamellae structure, and the difference is that the last aggregate is helix, in detail, three coupled helixes. Under the condition of $\alpha_{AW} = \alpha_{BW} = \alpha_{CW} = 120$, all formed lamella-like morphologies in Figures 2b and 7b also have the similar dynamic evolution process. For l-$A_2B_2C_2$ in $\boldsymbol{R} = 60$ and $\alpha_{AW} = 50$, $\alpha_{W} = 25$, and $\alpha_{CW} = 120$, block B first aggregates several small balls, then go through the fusion, and finally arrive at the morphology of a core plus the corona. Almost from the outset, block A forms the last phase that is an irregular lump, and the corresponding shape evolution always accompany the changeover of block C, which change from a cage to a broken cage.

4 Conclusions

In summary, we utilize DPD methods to explore the confinement-induced self-assembled morphologies of linear ABC triblock copolymers under the rigid spherical cavity and their dynamic evolution pathways. The interaction parameters between different blocks are fixed at $\alpha_{AB} = 45$, $\alpha_{AC} = 90$, and $\alpha_{BC} = 75$ to represent the famous μ-EOF triblock copolymers (41, 42), like our previous works (36, 40). Then large parameter spaces including three block sequences, seven block lengths, two radii of rigid spherical cavity, and five sets of α_{iW} are considered. Except for several novel nanostructures, such as multilayer onion, coupled helix, stacked lamella, cage, and so on, the effects of block sequence, wall selectivity, and spherical radius on the morphologies variation are stressed. For symmetric terpolymers, such as l-$A_2B_2C_2$, l-$A_2C_2B_2$, and l-$B_2A_2C_2$, only when block B locates at the middle, the morphology shows the significant difference no matter how the wall selectivity. For asymmetric terpolymers, such as l-$A_2B_8C_8$, l-$A_2C_8B_8$, l-$B_2A_8C_8$, and l-$B_2C_8A_8$, block sequences can provide the more effective influence on the morphological variety. In fact, the influence of wall selectivity is generally related to the position of blocks (i.e. block sequences). When the wall-preferred block is at the middle, the morphology of the corresponding terpolymer is very different to that formed by the wall-preferred block at the ends. At the same time, the block length and symmetry can also play a significant role. As for spherical radius, its influence on the morphology is clearly given in Figure 9. The main characteristic is that the spherical radius is larger than the block length; therefore, the triblock copolymers need alternatively fill the cavity, which results in the formation of multilayer onion-like structures. If the cavity wall repels any one block, the effects of spherical radius nearly disappear, and the terpolymers are inclined to form the lamella or the helix. As a whole, based on the dynamics evolution of morphologies, we can know that all factors (block sequence, wall selectivity, spherical radius, and block radio/length) exert the influence on the self-assembly and morphology of linear ABC triblock copolymer almost simultaneously. Combining previous crucial works on confined self-assembly (5–18, 25, 26, 31, 35), the results in this work are helpful to understand the formation mechanism of valuable nanostructures from the self-assembly of linear ABC triblock copolymers under the rigid spherical confinement.

Acknowledgments: All the authors appreciate very much the financial support from CAEP Foundation (no. 2014-1-075), National Nature Sciences Foundation of China (no. 11402241), and Sichuan University of Science & Engineering Foundation (No. 2015RC28).

References

1. Hamley IW. Block copolymers in solution: fundamentals and applications. Hoboken, NJ: Wiley; 2005.
2. Savic MR, Luo L, Eisenberg A, Maysinger D. Micellar nanocontainers distribute to defined cytoplasmic organelles. Science 2003;300(5619):615–8.
3. Ruiz R, Kang H, Detcheverry FA, Dobisz E, Kercher DS, Albrecht TR, Pablo JJ, Nealey PF. Density multiplication and improved lithography by directed block copolymer assembly. Science 2008;321(5891):936–9.
4. Bates FS, Fredrickson GH, Hucul D, Hahn SF. PCHE-based pentablock copolymers: evolution of a new plastic. AIChE J. 2001;47(4):762–5.
5. He X, Song M, Liang HJ, Pan CY. Self-assembly of the symmetric diblock copolymer in a confined state: Monte Carlo simulation. J Chem Phys. 2001;114(23):10510–9.
6. Zhang L, Liu C, Shang H, Cao X, Chai S, Chen Q, Wu L, Li H. Electrostatic tuning of block copolymer morphologies by inorganic macroions. Polymer 2016;106(5):53–61.
7. Yu B, Li B, Jin Q, Ding D, Shi AC. Self-assembly of symmetric diblock copolymers confined in spherical nanopores. Macromolecules 2007;40(25):9133–42.
8. Zhu Y, Jiang W. Self-assembly of diblock copolymer mixtures in confined states: a monte carlo study. Macromolecules 2007;40(8):2872–81.

9. Chen P, Liang H, Shi AC. Microstructures of a cylinder-forming diblock copolymer under spherical confinement. Macromolecules 2008;41(22):8938–43.
10. Tanaka T, Saito N, Okubo M. Control of layer thickness of onion-like multilayered composite polymer particles prepared by the solvent evaporation method. Macromolecules 2009;42(19): 7423–29.
11. Yan N, Zhu Y, Jiang W. Self-assembly of AB diblock copolymer confined in a soft nano-droplet: a combination study by Monte Carlo simulation and experiment. J Phys Chem B. 2016;120(46):12023–9.
12. Yan N, Liu H, Zhu Y, Jiang W, Dong Z. Entropy-driven hierarchical nanostructures from cooperative self-assembly of gold nanoparticles/block copolymers under three-dimensional confinement. Macromolecules 2015;48(16):5980–7.
13. Shi AC, Li B. Self-assembly of diblock copolymers under confinement. Soft Matter. 2013;9(5):1398–413.
14. Yu B, Deng J, Li B, Shi AC. Patchy nanoparticles self-assembled from linear triblock copolymers under spherical confinement: a simulated annealing study. Soft Matter. 2014;10(35):6831–43.
15. Sheng Y, An J, Zhu Y. Self-assembly of ABA triblock copolymers under soft confinement. Chem Phys. 2015;452:46–52.
16. Su YJ, Ma ZX, Huang JH. Simulation study on the assembly of rod-coil diblock copolymers within coil-selective nanoslits. e-Polymers 2016;16(4):343–9.
17. Yan N, Zhu Y, Jiang W. Self-assembly of ABC triblock copolymers under 3D soft confinement: a Monte Carlo study. Soft Matter. 2016;12:965–72.
18. Yu B, Sun P, Chen T, Jin Q, Ding D, Li B, Shi AC. Confinement-induced novel morphologies of block copolymers. Phys Rev Lett. 2016;96(13):138306.
19. Zhou Y, Xia HG, Long XP, Xue XG, Qian W. Complex multicompartment micelles from simple ABC linear triblock copolymers in solution. Macromol Theory Simul. 2015;24(2):85–8.
20. Zhou Y, Zhou C, He X, Xue XG, Qian W, Luo SK, Xia HG. Shear-induced self-assembly of linear ABC triblock copolymers in solution: creation of 1D cylindrical micellar structures. RSC Adv. 2016;6(7):5711–7.
21. Ludwigs S, Schmid K, Stafford CM, Amis EJ, Fasolka MJ, Karim A, Magerle R, Krausch G. Combinatorial mapping of the phase behavior of ABC triblock terpolymers in thin films: experiments. Macromolecules 2005;38(5):1850–8.
22. Tang CB, Bang J, Stein GE, Fredrickson GH, Hawker CJ, Kramer EJ, Sprung M, Wang J. Square packing and structural arrangement of ABC triblock copolymer spheres in thin films. Macromolecules 2008;41(12):4328–39.
23. Dobriyal P, Xiang HQ, Kazuyuki M, Chen JT, Jinnai H, Russell TP. Cylindrically confined diblock copolymers. Macromolecules 2009;42(22):9082–8.
24. Arsenault AC, Rider DA, Tetreault N, Chen JL, Coombs N, Ozin GA, Manners I. Block copolymers under periodic, strong three-dimensional confinement. J Am Chem Soc. 2005;127(28):9954–5.
25. Xu JP, Yang Y, Wang K, Li JY, Zhou HM, Xie X L, Zhu JT. Structural transformation of diblock copolymer/homopolymer assemblies by tuning cylindrical confinement and interfacial interactions. Langmuir 2015;31(45):12354–61.
26. Yabu H, Higuchi T, Jinnai H. Frustrated phases: polymeric self-assemblies in a 3D confinement. Soft Matter. 2014;10(17):2919–31.
27. Geisinger T, Müller M, Binder K. Symmetric diblock copolymers in thin films. I. Phase stability in self-consistent field calculations and Monte Carlo simulations. J Chem Phys. 1999;111(11):5241–7.
28. Yang YZ, Qiu F, Zhang HD, Yang YL. Cylindrical phase of diblock copolymers confined in thin films. A real-space self-consistent field theory study. Polymer 2006;47(6):2205–16.
29. Ludwigs S, Krausch G, Magerle R, Zvelindovsky AV, Sevink GJA. Phase behavior of ABC triblock terpolymers in thin films: mesoscale simulations. Macromolecules 2005;38(5):1859–67.
30. Chen HY, Fredrickson GH. Morphologies of ABC triblock copolymer thin films. J Chem Phys. 2002;116(3):1137–6.
31. Li SB, Jiang Y, Chen JZY. Morphologies and phase diagrams of ABC star triblock copolymers confined in a spherical cavity. Soft Matter 2013;9(19):4843–54.
32. Arai N, Yausoka K, Zeng XC. Self-assembly of triblock Janus nanoparticle in nanotube. J Chem Theory Comput. 2013;9(1):179–87.
33. Chi P, Wang Z, Li BH, Shi AC. Soft confinement-induced morphologies of diblock copolymers. Langmuir 2011;27(18):11683–9.
34. Sheng YP, An J, Zhu YT. Self-assembly of ABA triblock copolymers under soft confinement. Chem Phys. 2015;452(1):46–52.
35. Chang HY, Chen YF, Sheng YJ, Tsao HK. Blending-induced helical morphologies of confined linear triblock copolymers. J Taiwan Inst Chem E. 2015;56(5):196–200.
36. Zhou Y, Long XP, Xue XG, Qian W, Zhang CY. Morphologies and dynamics of linear ABC triblock copolymers with different block sequences. RSC Adv. 2015;5(10):7661–4.
37. Hoogerbrug PJ, Koelman JMVA. Simulating microscopic hydrodynamic phenomena with dissipative particle dynamics. Europhys Lett. 1992;19(3):155–9.
38. Espanol P, Warren PB. Statistical mechanics of dissipative particle dynamics. Europhys Lett. 1995;30(4):191–9.
39. Groot RD, Warren PB. Dissipative particle dynamics: bridging the gap between atomistic and mesoscopic simulation. J Chem Phys. 1997;107(11):4423–36.
40. Zhou C, Xia HG, Zhou Y, Xue XG, Luo SK. Dissipative particle dynamics simulations of the morphologies and dynamics of linear ABC triblock copolymers in solutions. RSC Adv. 2015;5(71):58024–31.
41. Li Z, Kesselman E, Talmon Y, Hillmyer MA, Lodge TP. Multicompartment micelles from ABC miktoarm stars in water. Science 2004;306(5963):98–101.
42. Xia J, Zhong C. Dissipative particle dynamics study of the formation of multicompartment micelles from ABC star triblock copolymers in water. Macromol Rapid Commun. 2006;27(14):1110–4.